Hyper-Truncated *N*-Acetyl-β-D-Glucosamine Decorations Augment the Activity and Inhibition Potential of Neutrophil Granule Myeloperoxidase

Harry C. Tjondro[1,2], Julian Ugonotti[1,2]*, Rebeca Kawahara[1,2]*, Sayantani Chatterjee[1,2]*, Ian Loke[3], Siyun Chen[4], Fabian Soltermann[4], Hannes Hinneburg[1,2], Benjamin L. Parker[5], Vignesh Venkatakrishnan[6], Regis Dieckmann[6], Oliver C. Grant[7], Johan Bylund[8], Alison Rodger[1,2], Robert J. Woods[7], Weston B. Struwe[4], Anna Karlsson-Bengtsson[6,9], Morten Thaysen-Andersen[1,2#]

[1]*Department of Molecular Sciences, Macquarie University, Sydney, NSW, Australia*

[2]*Biomolecular Discovery Research Centre, Macquarie University, Sydney, NSW, Australia*

[3]*Cordlife Group Limited, Singapore, Singapore*

[4]*Physical and Theoretical Chemistry, Department of Chemistry, University of Oxford, Oxford, United Kingdom*

[5]*Department of Physiology, University of Melbourne, Melbourne, VIC, Australia*

[6]*Department of Rheumatology & Inflammation Research, Institute of Medicine, Sahlgrenska Academy, University of Gothenburg, Gothenburg, Sweden*

[7]*Complex Carbohydrate Research Center, University of Georgia, Athens, United States*

[8]*Department of Oral Microbiology and Immunology, Institute of Odontology, Sahlgrenska Academy, University of Gothenburg, Gothenburg, Sweden, Sweden*

[9]*Department of Biology and Biological Engineering, Chalmers University of Technology, Gothenburg, Sweden*

*****Contributed equally*

Running title: The Sugar Code of Neutrophil Myeloperoxidase

Keywords: Myeloperoxidase, *N*-glycosylation, *N*-acetyl-β-D-glucosamine, neutrophil, granule, processing, activity, inhibition, ceruloplasmin, granulopoiesis, degranulation

[#]**Corresponding author**:
Dr Morten Thaysen-Andersen, PhD
Department of Molecular Sciences
Macquarie University
NSW-2109, Sydney, Australia
Phone: +61 2 9850 7487 / Email: morten.andersen@mq.edu.au

Abbreviations

AUC, area-under-the-curve; Az granule, azurophilic granule; Az-MPO, azurophilic granule-resident MPO; BN, band neutrophil; CD, circular dichroism; CytB/I, cytochalasin B and ionomycin; Dg-MPO, degranulated MPO; EIC, extracted ion chromatogram; Endo H, endoglycosidase H; Fuc (F), α-L-fucose; Ge granule, gelatinase granule; Ge-MPO, gelatinase granule-resident MPO; GlcNAc, *N*-acetyl-β-D-glucosamine; H_2O_2, hydrogen peroxide; HOCl, hypochlorous acid; LC-MS/MS, liquid chromatography tandem mass spectrometry; LDH, lactate dehydrogenase; Man, α/β-D-mannose; MD, molecular dynamics; MM, metamyelocyte; MOI, multiplicity-of-infection; MPO, myeloperoxidase; nMPO, neutrophil-derived myeloperoxidase (unfractionated); PDB, Protein Data Bank; PM, promyelocyte; PMN, polymorphonuclear cell (neutrophil); RMSD, root mean square deviation; RMSF, root mean square fluctuation; SD, standard deviation; Se/Pl, secretory vesicle and plasma membrane fraction; Se/Pl-MPO, secretory vesicle/plasma membrane-resident MPO; SN, neutrophil with segmented nuclei; Sp granule, specific granule; Sp-MPO, specific granule-resident MPO; TMB, 3,3’,5,5’-tetramethylbenzidine.

Abstract

Myeloperoxidase (MPO), an important glycoprotein in neutrophil-mediated immunity, produces microbicidal hypohalous acids, but the underpinning glycobiology remains elusive. Deep characterisation of neutrophil-derived MPO (nMPO) using advanced mass spectrometry demonstrated that under-processed oligomannosidic-, truncated paucimannosidic- and hyper-truncated *N*-acetyl-β-D-glucosamine (GlcNAc) core-type asparagine-linked glycans decorate the protein. Occlusion of Asn355 and Asn391 and sterical hindrance of Asn323- and Asn483-glycans located in the MPO dimerisation zone were found to shape the local glycan processing thereby providing a molecular basis for the site-specific nMPO glycosylation. Native mass spectrometry, mass photometry, and glycopeptide profiling revealed extreme molecular complexity of dimeric nMPO arising from heterogeneous glycosylation, oxidation, chlorination and polypeptide truncation variants, and a lower-abundance monomer. Longitudinal profiling of maturing, mature, granule-separated, and pathogen-activated neutrophils demonstrated that MPO is dynamically expressed during granulopoiesis, unevenly distributed across granules and rapidly degranulated, but surprisingly carries uniform glycosylation across conditions. Complete proMPO-to-MPO maturation evidently occur during early/mid-stage granulopoiesis. The conserved Asn355- and Asn391-sequons displayed elevated GlcNAc signatures and higher oxidation and chlorination activity of the secretory vesicle/plasma membrane-resident MPO relative to MPO from other granules. Endoglycosidase H-treated nMPO displaying Asn355-/Asn391-GlcNAcylation recapitulated the activity gain and showed increased thermal stability and enhanced polypeptide flexibility relative to untreated nMPO as measured by activity assays, circular dichroism and molecular dynamics. Endoglycosidase H-treated nMPO also demonstrated an elevated ceruloplasmin-mediated inhibition relative to nMPO. Modelling revealed that hyper-truncated Asn355-glycans positioned in the MPO:ceruloplasmin interface are critical for contact-free inhibition. We report on novel roles of the peculiar MPO glycosylation providing new insight into neutrophil glycobiology.

Introduction

The myeloid lineage-specific myeloperoxidase (MPO) is a heavily glycosylated dimeric protein produced exclusively by neutrophils and monocytes. Facilitated by its peroxidase activity, MPO catalyses the formation of highly reactive oxidation products including hypochlorous acid (HOCl) from chloride ions (Cl^-) and hydrogen peroxide (H_2O_2), substrates found in the maturing phagosomes (Davies et al., 2008; Klebanoff, 2005). From the principal residence in the azurophilic (Az) granules and to a lesser extent in the specific (Sp) and gelatinase (Ge) granules, and in secretory vesicles and the plasma membrane (Se/Pl) of neutrophils (Borregaard and Cowland, 1997; Rørvig et al., 2013), MPO reaches the maturing phagosome via heterotypic fusion or is degranulated upon neutrophil activation (Bjornsdottir et al., 2016; Borregaard et al., 2007). In the phagosome, MPO generates highly reactive hypohalous acids and nitrogen dioxide, which readily react to form diverse reactive oxygen species, key microbicidal and immune-regulatory products of the neutrophil MPO-halide system.

Our knowledge of MPO has improved considerably over the past decades (Agner, 1958; Harrison and Schultz, 1976; Klebanoff, 1968). New fascinating facets of the immensely complex MPO biology continue to emerge (Delporte et al., 2018; Nauseef, 2018; Vanhamme et al., 2018). MPO is an essential component of the innate immune system. MPO-deficient individuals show reduced abilities to fight invading pathogens (Aratani et al., 2006; Takeuchi et al., 2012). As recently reviewed (Khan et al., 2018), MPO is also involved in many pathologies including cardiovascular diseases (Cheng et al., 2019; Kim et al., 2018), rheumatoid arthritis (Stamp et al., 2012). and multiple sclerosis (Gray et al., 2008).

The complex biogenesis and maturation of MPO have been intensely studied (Grishkovskaya et al., 2017; Nauseef, 2018). In brief, human MPO is translated as a single 80 kDa signal peptide-containing polypeptide chain. This preproMPO form undergoes extensive proteolytic processing including, firstly, the removal of the signal peptide to form apoproMPO. The enzymatically active proMPO form is rapidly generated by heme acquisition in the endoplasmic reticulum (Nauseef et al., 1992). Protease-driven polypeptide processing then efficiently removes the propeptide and an internal hexapeptide, which separates the light (α, 12.5 kDa) and heavy (β, 60-65 kDa) chains that remain covalently linked via the catalytic heme (see Figure 3E for schematics). His261 and Arg405 (UniProtKB numbering) are key catalytic residues of the active site that is formed around the heme moiety positioned between the α-

and β-chains. Presumably within the Golgi, the α- and β-chains are further processed and extensively post-translationally modified before and/or after the formation of the mature MPO diprotomer (ααββ, ~150 kDa) that is joined by a Cys319-Cys319 bridge.

The high-resolution crystal structures of neutrophil-derived MPO (nMPO) with and without cognate and artificial ligands have considerably improved our knowledge of the secondary, tertiary and quaternary structure of MPO, the position of the heme and other hetero-atoms essential for enzymatic activity (e.g. Ca^{2+}), and the interactions to the endogenous inhibitor ceruloplasmin (Blair-Johnson et al., 2001; Carpena et al., 2009; Fiedler et al., 2000; Grishkovskaya et al., 2017; Samygina et al., 2013). Nauseef and colleagues reported already 30 years ago on the existence of five sequons for asparagine-linked (*N*-linked) glycosylation (Asn323, Asn355, Asn391, Asn483, Asn729) all located within the mature MPO β-chain (Nauseef, 1986, 1987). Most MPO crystal structures harbour remnants of *N*-glycan moieties, but our structural knowledge of the MPO glycosylation remains immature since complex carbohydrates are usually incompletely resolved with X-ray crystallography.

Three glycoanalytical studies have reported on nMPO glycosylation (Ravnsborg et al., 2010; Reiding et al., 2019; Van Antwerpen et al., 2010). In those studies, mass spectrometry-based glycopeptide analyses were used to obtain important site-specific information of the monosaccharide compositions conjugated to nMPO. Compositions corresponding to peculiar chitobiose core-, paucimannosidic-, oligomannosidic- and complex-type *N*-glycans were reported, but neither the glycan fine structures and occupancy at each site nor the biosynthesis and functional relevance of the *N*-glycans carried by nMPO distributed across the neutrophil granules were addressed. In fact, molecular-level knowledge of the roles of nMPO glycosylation is critically missing despite recent reports suggesting E-selectin binding (Silvescu and Sackstein, 2014), antigenicity (Wang et al., 2018; Yu et al., 2017), and modulation of the enzyme activity (Van Antwerpen et al., 2010) of the MPO glycans.

We are here the first to characterise the deep structure-biosynthesis-activity relationship of nMPO and to longitudinally profile the dynamic expression, protein processing and site-specific glycosylation of MPO from maturing, mature, granule-separated and activated neutrophils. Multi-omics strategies were used to obtain new molecular-level insight into the intriguingly complex sugar code of MPO of importance to fundamental neutrophil glycobiology and MPO-mediated immune processes.

Experimental Procedures

Donors, Neutrophil Handling, Granule Fractionation, and Neutrophil-Derived MPO

Buffy coats of healthy individuals (Donor a-i) were collected at The Blood Center, Sahlgrenska University Hospital, Gothenburg, Sweden, see **Supplementary Table S1** for sample overview. Resting neutrophils (>99%/95% viability/purity) were isolated (Clemmensen et al., 2014; Rørvig et al., 2013). See **Extended Methods** (SI) for details of all experiments.

Neutrophil granules were separated using nitrogen cavitation and Percoll separation. Three-layered Percoll separation (Donor c-f) separated the Az, Sp, and Ge granules and the Se/Pl fraction while two-layered Percoll separation (Donor a-b) fractionated Az from Sp/Ge granules and Se/Pl fractions as validated using granule markers (Feuk-Lagerstedt et al., 2007). Granules were lysed and proteins collected (Clemmensen et al., 2014; Nauseef, 2014a).

Resting neutrophils (Donor g-i) were inoculated with *Staphylococcus aureus* (LS1, multiplicity-of-infection (MOI) 5:1, neutrophil:bacteria), 37°C, 0-120 min. Activation controls without *S. aureus* and with cytochalasin B/ionomycin (CytB/I) stimulation, and Triton-X 100-based cell death controls were included. Degranulation of MPO (Dg-MPO) and cell death were monitored longitudinally in supernatant fractions using ELISA (ICL LAB) and lactate dehydrogenase (LDH) release using the Cytotoxicity Detection KitPLUS (Sigma).

Protein and transcript data of maturing neutrophils including promyelocytes (PMs), metamyelocytes (MMs), band neutrophils (BNs), neutrophils with segmented nuclei (SNs), and circulating polymorphonuclear cells (PMNs, resting neutrophils, included as a study reference) were obtained by re-interrogation of published data (Hoogendijk et al., 2019).

Human neutrophil-derived MPO (nMPO, UniProtKB, P05164, >95% purity) was from pooled donor blood (Lee BioSolutions). The purity, concentration, structural integrity and enzyme activity of nMPO was confirmed prior to analysis (see below).

Glycan Profiling

N-glycans were released from nMPO using *Elizabethkingia miricola* peptide-*N*-glycosidase F (Promega) (Jensen et al., 2012). Reduced *N*-glycans were profiled in technical triplicates using porous graphitised carbon liquid chromatography-tandem mass spectrometry (LC-MS/MS) in negative ion polarity on an LTQ Velos Pro ion trap mass spectrometer (Thermo Scientific)

(Hinneburg et al., 2019). Glycan fine structures were manually elucidated (Abrahams et al., 2018; Everest-Dass et al., 2013). RawMeat v2.1 (Vast Scientific) and GlycoMod (Expasy) aided the process. The *N*-glycan distribution was established from area-under-the-curve (AUC) measurements of extracted ion chromatograms (EICs) using Skyline v20.1.0.76 (Ashwood et al., 2018).

Glycopeptide Profiling

Glycopeptides and peptides were profiled from i) nMPO, ii) monomer(αβ)-dimer(ααββ)-separated nMPO, iii) endoglycosidase H- (Endo H-) treated and untreated nMPO, iv) granule-separated MPO, and v) Dg-MPO released from pathogen-activated neutrophils. For i) Reduced and carbamidomethylated nMPO was digested in technical triplicates using sequencing-grade porcine trypsin (Promega), ii) Monomeric and dimeric nMPO were separated using cooled non-reductive SDS-PAGE. Protein bands were in-gel trypsin digested, iii) Endo H-treated and untreated nMPO (see below) were applied separately to SDS-PAGE. The β-chains (53-58 kDa) were in-gel trypsin digested, iv) Isolated granule fractions were briefly introduced into SDS-PAGE gels. Bands containing all granule proteins were in-gel trypsin digested, and v) Released proteins were acetone precipitated, reduced, alkylated, and in-solution trypsin digested. All peptide mixtures were desalted before LC-MS/MS.

Peptides were separated using C18 chromatography and detected using a Q-Exactive HF-X Hybrid Quadrupole-Orbitrap mass spectrometer (Thermo Scientific) in positive ion polarity. LC-MS/MS data were searched against the canonical human MPO (P05164) and/or the human proteome (reviewed UniProtKB entries) using multiple search strategies employing Byonic v3.6.0 (Protein Metrics) and MaxQuant v1.6, see **Supplementary Table S2** for overview. Variable modifications including Met and Trp mono-/di-oxidation, Tyr mono-/di-chlorination and *N*-glycan libraries were included in the searches. Glycopeptides with Byonic PEP-2D scores < 0.001 were considered and manually validated (Kawahara et al., 2018). Non-glycan modified peptides were filtered to peptide-to-spectral matches and protein false discovery rates < 0.01-0.03 (MaxQuant) or PEP-2D scores < 0.001 (Byonic). Glycopeptides were profiled based on AUCs of monoisotopic EICs of glycopeptide precursors using Skyline v20.1.0.76 or XCalibur v2.2 (Thermo Scientific). Other peptides and proteins were quantified based on precursor intensities using MaxQuant (Cox and Mann, 2008).

Intact nMPO Analysis using Native MS and Mass Photometry

Top down/native MS was performed of i) the intact α-chain of nMPO and ii) intact nMPO. For, i) nMPO was reduced, desalted and injected on a C4 LC column connected to an Agilent 6538 quadrupole-time-of-flight mass spectrometer operating in high-resolution positive polarity mode. Mass spectra were deconvoluted with MassHunter vB.06 (Agilent Technologies). Assignments were guided by the LC-MS/MS peptide data, see **Supplementary Table S3A**, and ii) Intact nMPO was infused into a modified Q-Exactive (Thermo Scientific) operating in positive ion polarity via nano-ESI using custom-made gold-coated capillaries (Gault et al., 2016). Data were processed with XCalibur v2.2 (Thermo Scientific), spectra deconvoluted with UniDec (Marty et al., 2015), and annotated using in-house software.

Intact nMPO was analysed using single-molecule mass photometry (Soltermann et al., 2020). Coverslips were assembled for delivery using silicone CultureWell gaskets (Grace Bio-Labs). Data were acquired, processed and analysed using custom software (Young et al., 2018).

Visualisation, Modelling, Molecular Dynamics, Solvent Accessibility, and Sequence Alignments

The structure of human dimeric MPO obtained by X-ray crystallography (PDBID, 1D2V) was visualised using PyMOL Molecular Graphic System v2.3 (Schrödinger) and used for modelling. Signature *N*-glycans were added *in silico* using the Carbohydrate and Glycoprotein builders within GLYCAM-Web (http://glycam.org) to mimic nMPO (WT), Endo H-treated nMPO (P1), the hyper-truncated Asn355-/Asn391-glycophenotype elevated in Se/Pl-MPO (P2) and an MPO glycoform with semi-truncated glycans at Asn355 and Asn391 (P3), see **Supplementary Table S4**. The per-residue solvent accessibilities, root mean square deviation/fluctuation (RMSD/RMSF) and secondary structures were calculated using Cpptraj (AmberTools 18), plotted with Gnuplot 5.2 and visualised using VMD 1.9.3. Snapshots from the molecular dynamics (MD) simulations of WT- and P1-MPO were structurally aligned to the structure available for the ceruloplasmin-MPO complex (4EJX) via the MPO protein backbone.

Five crystal structures of MPO (1D2V, 1CXP, 1DNU, 1DNW, 5FIW) were used to assess the relative solvent accessibilities to the Asn residue of all sequons of monomeric MPO and to the β1,2-GlcNAc of FA1-glycans linked to Asn323, Asn483 and Asn729 of monomeric and dimeric MPO using NACCESS (5 Å radii probe) (Hubber and Thornton, 1993).

Sequence alignments of human MPO (P05164) to i) the family of human peroxidases including eosinophil peroxidase (EPO, P11678), lactoperoxidase (LPO, P22079) and thyroid peroxidase (TPO, P07202), and ii) MPO from key mammalian species including mouse MPO (P11247), macaque MPO (F7BAA9), porcine MPO (K7GRV6) and bovine MPO (A6QPT4, all downloaded July 2020) were performed using T-Coffee (http://tcoffee.crg.cat/apps/tcoffee) and Boxshade (http://www.ch.embnet.org/software/BOX_form).

Endoglycosidase H-Treatment of nMPO

Intact nMPO was incubated with or without *Streptomyces plicatus* endoglycosidase H (Endo H, Promega) under native conditions. All samples including controls containing only Endo H were used immediately for activity and inhibition profiling and structural characterisation.

Chlorination and Oxidation Activity and Ceruloplasmin Inhibition of MPO

Chlorination activities of various MPO glycoforms and controls were determined by the formation of HOCl captured via taurine per time using HOCl standard curves (activity assay 1) (Dypbukt et al., 2005). Reactions were initiated by sequential addition of taurine and H_2O_2 (Sigma), stopped by catalase (Sigma) and measured at 650 nm after addition of 3,3′,5,5′-tetramethylbenzidine (TMB, Sigma). Relative oxidation activities of various MPO glycoforms and controls were determined using a TMB assay (activity assay 2) and an *o*-phenylenediamine (OPD) assay (activity assay 3). Reactions were initiated by the addition of TMB or OPD (Sigma), quenched after incubation with sulphuric acid (Sigma) and the colour intensity measured at 450 nm or 492 nm, respectively. Readings were adjusted based on water and Endo H controls, **Supplementary Table S5**.

Ceruloplasmin-mediated inhibition of the MPO enzyme activity was determined using activity assay 1-3. Endo H-treated and untreated nMPO and controls were incubated with and without human serum-derived ceruloplasmin (P00450, Lee BioSolutions) in technical triplicates prior to activity measurements. Readings were adjusted based on water, Endo H and ceruloplasmin controls.

Circular Dichroism Profiling and Temperature Stability

Circular dichroism (CD) data of nMPO, Endo H-treated nMPO and controls were collected in technical duplicates using 1 mm-pathlength cuvettes (Starna Scientific) in a Jasco J-1500 spectropolarimeter. CD spectra were recorded using 260–190 nm scans at pre-melting temperatures (20–50°C). Thermal stability was determined by monitoring the 208 nm signal over a temperature range. Readings were adjusted based on water and Endo H controls.

Data Representation and Statistics

Significance was tested using one-/two-tailed paired/unpaired Student's t-tests. Confidence was designated by $*p < 0.05$, $**p < 0.01$, $***p < 0.005$, $****p < 0.001$, $*****p < 0.0005$. ns, non-significant test ($p \geq 0.05$). Biological and technical (sample or analytical) replicates were stated. Data points were plotted as the mean and all error bars represent their standard deviation (SD).

Results and Discussion

Deep Characterisation of Neutrophil-Derived Myeloperoxidase

The heme-containing MPO (ααββ) adopts a complex dimeric structure comprising two identical αβ protomers, **Figure 1A**. Each β-chain harbours five sequons (Asn323, Asn355, Asn391, Asn483, Asn729) enabling extensive *N*-glycosylation of the MPO protein surface. The extreme molecular complexity of MPO remains incompletely characterised despite significant efforts (Ravnsborg et al., 2010; Reiding et al., 2019; Van Antwerpen et al., 2010).

To this end, we first applied glycomics to define with isomer resolution the fine structures of the heterogeneous *N*-glycan population decorating neutrophil-derived MPO (nMPO), **Figure 1B, Supplementary Figure S1, Supplementary Table S6** and **Supplementary Data S1**. Peculiar monoantennary complex-type (FA1G1S1a), under-processed oligomannosidic (M5-M6), truncated paucimannosidic (M2Fa-M3F) and hyper-truncated chitobiose core-type (GlcNAc1-GlcNAc1F) structures were found to be characteristic *N*-glycans of nMPO congruent with structures reported from neutrophil granules (Venkatakrishnan et al., 2020) and similar to the *N*-glycans carried by other granule-resident glycoproteins including neutrophil cathepsin G and elastase (Loke et al., 2017; Loke et al., 2015; Thaysen-Andersen et al., 2015). No *O*-linked glycans were detected.

Many non-glycan nMPO modifications including 18 Met and 9 Trp mono-/di-oxidations, two sites for Tyr mono-chlorination and several polypeptide truncation variants of both the α- and β-chains were identified using sensitive peptide-based profiling facilitating a near-complete sequence coverage of nMPO (α-/β-chain, 100.0%/99.8%), **Figure 1C**, **Supplementary Figure S2** and **Supplementary Data S2A-B**. Polypeptide hyper-oxidation, previously suggested to arise from the reactive oxidising agents produced by MPO (Ravnsborg et al., 2010), plays recognised roles in neutrophil function (Winterbourn et al., 2016). Further, site-specific glycoprofiling revealed an extensive micro- and macro-heterogeneity of all five *N*-glycosylation sites of nMPO, **Figure 1D**, **Supplementary Figure S3, Supplementary Table S7** and **Supplementary Data S3A-E**. In excellent agreement with studies reporting on the site-specific monosaccharide compositions of nMPO (Ravnsborg et al., 2010; Reiding et al., 2019; Van Antwerpen et al., 2010), we found that Asn323 and Asn483 were predominantly occupied by paucimannosidic-type *N*-glycans (M2F-M3F), Asn355 and Asn391 carried oligomannosidic-

type *N*-glycans (M5-M6) while Asn729 was largely unoccupied or carried chitobiose core-type (GlcNAc1-GlcNAc1F) *N*-glycans.

Intact mass analysis revealed limited α-chain heterogeneity (12,350-12,550 Da) arising from relatively few polypeptide truncation and oxidation variants, presumably Met251 and Met253, as supported by peptide data, **Figure 1E** and **Supplementary Table S3A**. In contrast, native MS demonstrated an extreme molecular complexity of dimeric nMPO (ααββ, 141.5-148.0 kDa, apex 143,958 Da) that matched a published lower-resolution profile of intact nMPO (apex 144,180 Da) (Reiding et al., 2019) and a theoretical profile generated from ~300,000 expected proteoforms predicted based on quantitative (glyco)peptide data (140.5-147.0 kDa), **Figure 1F** and **Supplementary Table S3B**). Native MS also indicated the existence of an nMPO monomer with a slightly lower-than-expected molecular mass (αβ, 70-73 kDa, data not shown). Cooled non-reductive SDS-PAGE followed by peptide profiling supported the presence of a maturely processed low-abundance nMPO monomer, **Supplementary Figure S4**. Single-molecule mass photometry, a technique capable of quantifying the stoichiometry, binding affinities and kinetics of protein complexes (Haussermann et al., 2019; Soltermann et al., 2020; Young et al., 2018), confirmed that nMPO exists both as a low-abundance monomer (αβ, 7%) and high-abundance dimer (ααββ, 93%) with an apparent monomer-dimer K_d of ~50 pM, **Figure 1G**. The biological role(s) of the maturely processed MPO monomer, which differs from the secreted monomeric proMPO reportedly elevated in blood in cardiovascular disease (Gorudko et al., 2018; Khalilova et al., 2018), remains unknown.

Solvent Accessibility and Oligomerisation Impact the Local Processing of nMPO N-Glycans

The molecular basis for the perplexing site-specific *N*-glycosylation of nMPO was explored by firstly investigating the early-stage glycoprotein processing where MPO presumably traffic the Golgi as a fully folded monomer (Nauseef, 2018). Close associations between the Asn accessibility and the degree of *N*-glycan type processing and core fucosylation were identified, **Figure 2A, Supplementary Table S7** and **Supplementary Table S8A**. We have reported on an accessibility-driven site-specific *N*-glycan processing of other mammalian glycoproteins (Thaysen-Andersen and Packer, 2012). The relatively inaccessible Asn355 and Asn391 carried under-processed oligomannosidic-type and afucosylated *N*-glycans as opposed to the comparably more surface exposed sites (Asn323, Asn483, Asn729) (p = 3.5 x 10^{-13} and 5.7 x

10^{-13}, respectively) carrying significantly more processed *N*-glycans (p = 4.7 x 10^{-4} and 7.6 x 10^{-8}) and a higher level of core fucosylation (both p = 1.3 x 10^{-7}).

Exploration of the late-stage MPO processing within the *N*-glycan truncation pathway, a recently reported glycan-processing pathway highly active in neutrophils (Thaysen-Andersen et al., 2015; Tjondro et al., 2019), demonstrated that the Asn483-glycans (and partly Asn323-glycans) undergo less truncation relative to Asn729-glycans, **Figure 2Bi**. Interestingly, the lower removal efficiency of the outer β1,2-GlcNAc and α1,3-Man residues of Asn483-glycans relative to Asn729-glycans (p = 3.5 x 10^{-5} and 1.1 x 10^{-8}, respectively) correlated with a reduced β1,2-GlcNAc accessibility of Asn483-FA1 glycans upon MPO dimerisation (p = 7.6 x 10^{-5}), **Figure 2Bii-iv** and **Supplementary Table S8B**. The dimerisation-dependent occlusion of the Asn483-glycans could be observed by the contact between (and hence masking of) the Asn483-FA1 glycan and the protein surface of the other αβ-protomer, **Figure 2Bv**. Intuitively, occlusion of the Asn483-glycans restricts *N*-acetyl-β-hexosaminidase and lysosomal α-mannosidase, two key glycoside hydrolases of the truncation pathway (Tjondro et al., 2019), to access their glycan substrates and, in turn, less efficiently catalyse β1,2-GlcNAc and α1,3-Man removal of Asn483-FA1 glycans. The Asn323-glycan positioned near the dimer interface was partially affected by MPO dimerisation as indicated by the weakly impaired α1,3-Man removal of Asn323-glycans (p = 0.014, Asn323 vs Asn729). The dimerisation-dependent protection of the Asn323- and Asn483-glycans from hydrolase-mediated truncation was supported by glycopeptide profiling of gel-separated monomeric and dimeric nMPO, **Supplementary Figure S4A.** This analysis confirmed that the outer β1,2-GlcNAc of the Asn323- and Asn483-glycans was more efficiently removed of monomeric rather than dimeric nMPO (p = 0.013 and 0.032, respectively), **Supplementary Table S9A-B**. Similar protective effects could be observed for the Asn323-glycans of dimeric MPO exhibiting less α1,3-Man removal efficiency relative to monomeric MPO (p = 0.008). Importantly, similar processing of the Asn729-glycans distal to the dimerisation interface were observed of monomeric and dimeric nMPO ($p \geq 0.05$). Collectively, and in line with current literature (Nauseef, 2018), this data indicate that MPO dimerisation takes place immediately before or quickly after MPO arrives in the neutrophil granules, a maturation step that affects the processing of the Asn323- and Asn483-glycans positioned in proximity to the MPO dimer interface.

Dynamics, Distribution, Processing and Glycosylation of MPO Across Neutrophil Life Stages

Dynamic expression of MPO mRNA and protein during granulopoiesis was demonstrated based on data re-interrogation (Hoogendijk et al., 2019), **Figure 3A**. The targeting-by-timing model (Cowland and Borregaard, 2016) and the PM-stage-specific transcription of MPO collectively provided a molecular basis for the uneven granule distribution of MPO, **Figure 3B**. Our data confirmed that MPO predominantly resides in azurophilic (Az, 82.9%) granules, but the specific (Sp) and gelatinase (Ge) granules and the secretory vesicles/plasma membrane (Se/Pl) also contain MPO as previously reported (Rørvig et al., 2013). Neutrophils are known to release their proteinaceous granule content via degranulation upon chemical stimulation (Bjornsdottir et al., 2016). To expand on these findings, we longitudinally monitored the release and glycosylation patterns of degranulated MPO (Dg-MPO) upon neutrophil activation mediated by low-level short-term infection by pathogenic *S. aureus*, **Figure 3C**.

Site-specific glycoprofiling of MPO from maturing, mature (resting), granule-separated, and pathogen-activated neutrophils showed surprisingly uniform MPO glycosylation across the studied neutrophil life-stages and conditions, **Figure 3D**. Similar MPO glycosylation patterns of all five sites were observed across all granule types (correlation coefficients, $r > 0.95$), which, as expected, matched the glycosylation of unfractionated nMPO from resting neutrophils (PMN-nMPO, $r > 0.95$, see **Supplementary Figure S5** and **Supplementary Table S10** for all data). Given our recent glycomics-based report of granule-specific *N*-glycosylation of resting neutrophils (Venkatakrishnan et al., 2020) and the observation of uniform *N*-glycosylation of neutrophil elastase across granules (Loke et al., 2017), the similar *N*-glycosylation of MPO distributed across granules indicates that granule-specific glycosylation arises from the different protein populations residing in each granule type rather than from distinctly different glycosylation of similar protein population across granules. We are currently exploring the mechanisms causing granule-specific glycosylation using deep glycoproteomics of isolated neutrophil granules.

Equally interesting, the MPO glycoprofiling of maturing neutrophils, facilitated by data re-analysis (Hoogendijk et al., 2019), indicated that PM-MPO and MPO from all subsequent neutrophil development steps surprisingly carry fully processed *N*-glycosylation signatures at all sites ($r > 0.93$). Supporting an MPO maturation in early-stage granulopoiesis, longitudinal profiling of the proMPO-to-MPO conversion within maturing, mature, and granule-separated

neutrophils showed a near-complete pro- and hexapeptide removal from metamyelocyte-derived MPO (MM-MPO, ~1% proMPO) and from MPO of more advanced cellular maturation stages, **Figure 3E**. Our data could not discriminate between the apoproMPO and proMPO forms (without and with heme, respectively), but the unprocessed form observed in this study is likely proMPO since heme acquisition reportedly occurs rapidly in the endoplasmic reticulum (Nauseef et al., 1992). Taken together, our data indicate that the heavily processed MPO undergoes rapid glycan and polypeptide maturation upon expression at the PM-stage during granulopoiesis.

S. aureus-mediated activation of neutrophils performed at sub-stoichiometric infection levels to simulate weak infection levels and prevent cell lysis (MOI 1:5) demonstrated a rapid (30-120 min) time-dependent and cell death-independent degranulation of Dg-MPO, **Figure 3F**. The Dg-MPO carried similar glycosylation to PMN-nMPO ($r > 0.91$) indicating a glycoform-independent MPO degranulation process. It remains unknown if the weakly altered glycans observed at selected sites (e.g. Asn355, $r = 0.81$) functionally impact the pathogen-killing ability of MPO or result from technical variation of the analytically challenging site-specific profiling of MPO directly from biological mixtures (Thaysen-Andersen et al., 2016).

Sequence alignments showed that Asn355 and Asn391 are conserved sequons within the family of human peroxidases and within MPO expressed across mammalian species, **Figure 3G** and **Supplementary Figure S6.** The sequon conservation implies functional relevance of glycans at these sites. Interestingly, absence of glycosylation and hyper-truncated GlcNAcβAsn were found to be elevated features at Asn355 ($p = 9.2 \times 10^{-5}$ and 0.04, respectively, Se/Pl- vs Az-MPO) and Asn391 ($p = 0.022$ for GlcNAcβAsn) of Se/Pl-MPO relative to MPO from other granules, **Figure 3H**. It may be speculated that the minimal Asn355- and Asn391-glycosylation of Se/Pl-MPO arises from the action of endoglycosidase H- (Endo H-) and peptide:*N*-glycosidase F-like hydrolases e.g. di-*N*-acetylchitobiase (Q01459) and N(4)-(beta-*N*-acetylglucosaminyl)-L-asparaginase (P20933) and/or glycoside hydrolases of the truncation pathway that may be co-expressed and co-sorted with MPO trafficking to these compartments (Damme et al., 2010; Tjondro et al., 2019). Regardless of the underlying biosynthesis, the position-specific enrichment of peculiar glycan signatures in specific compartments of the neutrophil is intriguing and without precedence in the literature.

Hyper-Truncated Asn355- and Asn391-GlcNAc Allosterically Augments the MPO Activity

Given their spatial orientation, the MPO *N*-glycans are unlikely to interfere with the substrate-product exchange to the heme-containing catalytic site, **Figure 4Ai**. Hyper-oxidation of Met251, Met253 and Trp255 lining the catalytic site was observed indicating extensive self-oxidation that may impact MPO activity by possibly reconfiguring the active site, **Figure 4Aii**. Activity assays performed on crudely fractionated granules of Donor a-b neutrophils demonstrated that Se/Pl-MPO exhibits a higher chlorination activity (3.7-9.0-fold) and oxidation activity (5.0-51.5-fold, Se/Pl- vs Az-MPO) than MPO from other granules, **Figure 4Aiii** and **Supplementary Table S11**. In support, peptide analysis of granules fractionated with high resolution of Donor c-f neutrophils confirmed that Se/Pl-MPO exhibits a higher chlorination activity than MPO from other granules based on a higher Tyr chlorination level of the granule proteins (p = 4.7 x 10^{-3}, Se/Pl- vs Az-MPO), **Figure 4Aiv** and **Supplementary Table S12**.

Endo H-treatment of nMPO under native conditions produced an Asn355- and Asn391-GlcNAc-rich glycophenotype mimicking the enriched glycoforms of Se/Pl-MPO, **Figure 4Bi**. Biochemical characterisation validated that the oligomannose-rich Asn355- and Asn391-glycans were fully converted to GlcNAcβAsn while the processed *N*-glycans in other positions were Endo H-insensitive, **Supplementary Figure S7**. The Endo H-treated nMPO exhibited higher chlorination and oxidation activity than untreated nMPO as established using three activity assays (3.4-5.8-fold, all $p < 0.005$), **Figure 4Bii** and **Supplementary Table S5A-C**.

The molecular basis for the intriguing glycoform-dependent MPO activity was investigated using CD and MD simulations of relevant MPO glycoforms (WT and P1-P3), **Supplementary Table S4A-B**. Endo H-treated (P1) and untreated nMPO (WT) displayed indistinguishable secondary structure profiles rich in helical content as reported (Banerjee et al., 2011; Paumann-Page et al., 2013) based on CD and predictions based on MD data, **Figure 4C** and **Supplementary Table S13A-B**. Notably, the Endo H-treated nMPO showed a higher initial melting temperature (+72°C) than untreated nMPO (+60°C) as determined by $CD_{208\,nm}$, **Figure 4Di** and **Supplementary Table S13C**. Both glycoforms finished the transition by +88°C, though about half the helical structure remained at this temperature. Thus, our data suggested that Endo H-treated nMPO displays an enhanced thermal stability relative to untreated nMPO. Interestingly, MD data indicated that the relatively higher thermal stability of Endo H-treated

nMPO was accompanied by a significantly higher global polypeptide accessibility relative to nMPO, **Figure 4Dii** and **Supplementary Figure S8-S9**. Similar accessibility gains distributed throughout the polypeptide chains, but with particular "hot-spots" of dramatically enhanced accessibility C-terminal to Asn355 and Asn391 (labelled b-c) and distal to the heme and active site residues (i-ii, His261/Arg405), were observed for P2 (mimicking the Se/Pl-MPO-enriched glycoforms). The P3 control glycoform carrying semi-truncated *N*-glycans at Asn355 and Asn391 (M2-M3) did not show elevated accessibility relative to nMPO suggesting that minimal Asn355-/Asn391-glycosylation is required to allosterically impact the global MPO structure and augment activity. In support, prolonged contacts were consistently observed between the β1,4-GlcNAc and β1,4-Man of the trimannosylchitobiose core (Manβ1,4GlcNAcβ1,4GlcNAcβAsn) and the protein surfaces immediately C-terminal to Asn355 and Asn391 during the MD simulation of elongated (beyond GlcNAcβAsn) glycans at these positions (data not shown). Such glycan-protein contacts, which may modulate protein stability and structure, are particularly interesting given that Asn355 and Asn391 are positioned on flexible loops proximal to the active site. The MD data including RMSD-based mobility measurements, **Supplementary Figure S8D**, however, were insufficiently sensitive to unravel the molecular basis for the observed structure-activity relationships of glycosylated MPO in greater details, which, consequently, await future exploration.

Hyper-Truncated Asn355-Glycosylation Enhances Ceruloplasmin-Mediated MPO Inhibition

The impact of glycosylation on MPO inhibition by ceruloplasmin, an endogenous inhibitor of MPO (Chapman et al., 2013), was explored by comparing the relative activity of Endo H-treated and untreated nMPO in the absence and presence of serum-derived ceruloplasmin, **Figure 5A**. The Endo H-treatment completely converted the oligomannose-rich Asn355 and Asn391 to GlcNAcβAsn-containing sites while sites containing processed glycans (e.g. Asn323) were Endo H-insensitive, **Figure 5B** and **Supplementary Figure S7**. The chlorination and relative oxidation rates of Endo H-treated and untreated nMPO incubated with and without ceruloplasmin were determined using three activity assays, **Figure 5C** and **Supplementary Table S5D-F**. Activity 1 and 3 showed significant ceruloplasmin-mediated inhibition of Endo H-treated nMPO ($p = 3.8 \times 10^{-4}$ and 8.5×10^{-5}) while untreated nMPO exhibited weak to no ceruloplasmin-mediated inhibition. For activity assay 2, an unexplained activity gain was

experienced by untreated nMPO upon the addition of ceruloplasmin while this activity gain was quenched for the Endo H-treated nMPO. The molecular mechanisms underpinning the intriguing glycoform-dependent MPO inhibition by ceruloplasmin were explored using a structure of the ceruloplasmin-MPO complex (PDBID, 4EJX) and MD data of relevant nMPO glycoforms of Asn323, Asn355 and Asn391 proximal to the complex interface, **Figure 5D**. The modelling demonstrated that Asn355 is the only sequon positioned directly in the MPO:ceruloplasmin interface, and, importantly, that Asn355-M6 and not Asn355-GlcNAc sterically clashes with ceruloplasmin thereby providing a molecular basis for the glycoform-dependent MPO inhibition by ceruloplasmin.

Conclusions

We have characterised the structure-biosynthesis-activity relationship of neutrophil-derived MPO and longitudinally profiled the spatiotemporal expression, protein processing, site-specific glycosylation and degranulation of MPO from maturing, mature, granule-separated and pathogen-activated neutrophils from healthy donors. Powered by modern multi-omics tools, our quantitative and longitudinal data add important molecular-level knowledge to our growing understanding of the complex MPO biology governing many innate immune processes central to human health and disease (Nauseef, 2014b; Winterbourn et al., 2016).

Bottom-up and top-down approaches were used to unravel the molecular complexity displayed by the heavily glycosylated and post-translationally modified nMPO. Glycans rarely reported in human glycobiology but indeed common to neutrophils including the truncated paucimannosidic-type and hyper-truncated chitobiose core-type *N*-glycans (Tjondro et al., 2019) and elaborate oxidation, chlorination and polypeptide truncation variants were found to be molecular site-specific signatures of nMPO. The structural data presented herein align with and significantly expand from important literature on this topic (Ravnsborg et al., 2010; Reiding et al., 2019; Van Antwerpen et al., 2010). Molecular mechanisms contributing to the peculiar site-specific MPO glycosylation were established. Several protein factors including the spatial environment and dimerisation status were found to affect the local *N*-glycan processing producing a position-specific glycan-code, which intriguingly shape not only the MPO structure, but also the activity profile and inhibition potential of the glycoprotein. The rarely reported GlcNAcβAsn-type glycosylation was found to decorate MPO and was

demonstrated to be elevated at strategic sites important for the activity and ceruloplasmin-mediated inhibition of MPO residing within highly mobile compartments of neutrophils. Taken together, our data suggest that neutrophils dynamically produce, process, package, store, and, upon activation, release a perplexing repertoire of related MPO glycoforms displaying a continuum of activity and inhibition profiles. The strategically positioned Asn355-sequon carrying both hyper-truncated and elongated *N*-glycan appeared particularly important for the modulation of MPO activity and inhibition.

In conclusion, this study has provided new molecular-level insights into the intriguingly complex sugar code of MPO of importance to fundamental neutrophil glycobiology and MPO-mediated immune processes central to human health and disease.

Acknowledgements

HCT was supported by an Australian Cystic Fibrosis postgraduate studentship award and an international Macquarie University Research Excellence Scholarship (iMQRES). SC was supported by an iMQRES. JU was supported by a Macquarie University Research Excellence Scholarship (MQRES). RK was supported by an Early Career Fellowship from the Cancer Institute NSW. MTA was supported by a Macquarie University Safety Net Grant.

The late Professor Niels Borregaard is thanked for valuable ideas and discussions seeding this research.

Author contributions

Conception of research, HCT, MTA; Experimental design, HCT, RK, IL, RJW, WBS, JB, AKB, MTA; Experimental execution, HCT, JU, RK, SC, IL, SC, FS, HH, BLP, VV, RD, OCG, AR, WBS; Data analysis and interpretation: HCT, JU, RK, SC, IL, SC, FS, HH, BLP, VV, RD, OCG, AR, RJW, WBS, MTA; Manuscript writing and editing: HCT, JU, RK, SC, OCG, AR, WBS, JB, AKB, MTA.

Author declarations

No conflict of interest has been declared.

References

Abrahams, J.L., Campbell, M.P., and Packer, N.H. (2018). Building a PGC-LC-MS N-glycan retention library and elution mapping resource. Glycoconjugate Journal *35*, 15-29.

Agner, K. (1958). Crystalline myeloperoxidase. Acta Chemica Scandinavica *12*, 89-94.

Aratani, Y., Kura, F., Watanabe, H., Akagawa, H., Takano, Y., Ishida-Okawara, A., Suzuki, K., Maeda, N., and Koyama, H. (2006). Contribution of the myeloperoxidase-dependent oxidative system to host defence against Cryptococcus neoformans. Journal of Medical Microbiology *55*, 1291-1299.

Ashwood, C., Lin, C.-H., Thaysen-Andersen, M., and Packer, N.H. (2018). Discrimination of Isomers of Released N- and O-Glycans Using Diagnostic Product Ions in Negative Ion PGC-LC-ESI-MS/MS. Journal of The American Society for Mass Spectrometry *29*, 1194-1209.

Banerjee, S., Stampler, J., Furtmuller, P.G., and Obinger, C. (2011). Conformational and thermal stability of mature dimeric human myeloperoxidase and a recombinant monomeric form from CHO cells. Biochim Biophys Acta *1814*, 375-387.

Bjornsdottir, H., Welin, A., Dahlgren, C., Karlsson, A., and Bylund, J. (2016). Quantification of heterotypic granule fusion in human neutrophils by imaging flow cytometry. Data Brief *6*, 386-393.

Blair-Johnson, M., Fiedler, T., and Fenna, R. (2001). Human Myeloperoxidase: Structure of a Cyanide Complex and Its Interaction with Bromide and Thiocyanate Substrates at 1.9 Å Resolution. Biochemistry *40*, 13990-13997.

Borregaard, N., and Cowland, J.B. (1997). Granules of the Human Neutrophilic Polymorphonuclear Leukocyte. Blood *89*, 3503.

Borregaard, N., Sørensen, O.E., and Theilgaard-Mönch, K. (2007). Neutrophil granules: a library of innate immunity proteins. Trends in Immunology *28*, 340-345.

Carpena, X., Vidossich, P., Schroettner, K., Calisto, B.M., Banerjee, S., Stampler, J., Soudi, M., Furtmüller, P.G., Rovira, C., Fita, I.*, et al.* (2009). Essential role of proximal histidine-asparagine interaction in mammalian peroxidases. The Journal of biological chemistry *284*, 25929-25937.

Chapman, A.L., Mocatta, T.J., Shiva, S., Seidel, A., Chen, B., Khalilova, I., Paumann-Page, M.E., Jameson, G.N., Winterbourn, C.C., and Kettle, A.J. (2013). Ceruloplasmin is an endogenous inhibitor of myeloperoxidase. J Biol Chem *288*, 6465-6477.

Cheng, D., Talib, J., Stanley, C.P., Rashid, I., Michaelsson, E., Lindstedt, E.L., Croft, K.D., Kettle, A.J., Maghzal, G.J., and Stocker, R. (2019). Inhibition of MPO (Myeloperoxidase) Attenuates Endothelial Dysfunction in Mouse Models of Vascular Inflammation and Atherosclerosis. Arteriosclerosis, thrombosis, and vascular biology, Atvbaha119312725.

Clemmensen, S.N., Udby, L., and Borregaard, N. (2014). Subcellular Fractionation of Human Neutrophils and Analysis of Subcellular Markers. In Neutrophil Methods and Protocols, M.T. Quinn, and F.R. DeLeo, eds. (Totowa, NJ: Humana Press), pp. 53-76.

Cowland, J.B., and Borregaard, N. (2016). Granulopoiesis and granules of human neutrophils. Immunol Rev *273*, 11-28.

Cox, J., and Mann, M. (2008). MaxQuant enables high peptide identification rates, individualized p.p.b.-range mass accuracies and proteome-wide protein quantification. Nat Biotechnol *26*, 1367-1372.

Damme, M., Morelle, W., Schmidt, B., Andersson, C., Fogh, J., Michalski, J.C., and Lubke, T. (2010). Impaired lysosomal trimming of N-linked oligosaccharides leads to hyperglycosylation of native lysosomal proteins in mice with alpha-mannosidosis. Mol Cell Biol *30*, 273-283.

Davies, M.J., Hawkins, C.L., Pattison, D.I., and Rees, M.D. (2008). Mammalian heme peroxidases: From molecular mechanisms to health implications. Antioxid. Redox Signal. *10*, 1199-1234.

Delporte, C., Zouaoui Boudjeltia, K., Furtmueller, P.G., Maki, R.A., Dieu, M., Noyon, C., Soudi, M., Dufour, D., Coremans, C., Nuyens, V.*, et al.* (2018). Myeloperoxidase-catalyzed oxidation of cyanide to cyanate: A potential carbamylation route involved in the formation of atherosclerotic plaques? Journal of Biological Chemistry.

Dypbukt, J.M., Bishop, C., Brooks, W.M., Thong, B., Eriksson, H., and Kettle, A.J. (2005). A sensitive and selective assay for chloramine production by myeloperoxidase. Free Radic. Biol. Med. *39*, 1468-1477.

Everest-Dass, A.V., Abrahams, J.L., Kolarich, D., Packer, N.H., and Campbell, M.P. (2013). Structural Feature Ions for Distinguishing N- and O-Linked Glycan Isomers by LC-ESI-IT MS/MS. Journal of The American Society for Mass Spectrometry *24*, 895-906.

Feuk-Lagerstedt, E., Movitz, C., Pellme, S., Dahlgren, C., and Karlsson, A. (2007). Lipid raft proteome of the human neutrophil azurophil granule. Proteomics *7*, 194-205.

Fiedler, T.J., Davey, C.A., and Fenna, R.E. (2000). X-ray Crystal Structure and Characterization of Halide-binding Sites of Human Myeloperoxidase at 1.8 Å Resolution. Journal of Biological Chemistry *275*, 11964-11971.

Gault, J., Donlan, J.A.C., Liko, I., Hopper, J.T.S., Gupta, K., Housden, N.G., Struwe, W.B., Marty, M.T., Mize, T., Bechara, C.*, et al.* (2016). High-resolution mass spectrometry of small molecules bound to membrane proteins. Nature Methods *13*, 333.

Gorudko, I.V., Grigorieva, D.V., Sokolov, A.V., Shamova, E.V., Kostevich, V.A., Kudryavtsev, I.V., Syromiatnikova, E.D., Vasilyev, V.B., Cherenkevich, S.N., and Panasenko, O.M. (2018). Neutrophil activation in response to monomeric myeloperoxidase. Biochem Cell Biol *96*, 592-601.

Gray, E., Thomas, T.L., Betmouni, S., Scolding, N., and Love, S. (2008). Elevated activity and microglial expression of myeloperoxidase in demyelinated cerebral cortex in multiple sclerosis. Brain pathology (Zurich, Switzerland) *18*, 86-95.

Grishkovskaya, I., Paumann-Page, M., Tscheliessnig, R., Stampler, J., Hofbauer, S., Soudi, M., Sevcnikar, B., Oostenbrink, C., Furtmuller, P.G., Djinovic-Carugo, K.*, et al.* (2017). Structure of human promyeloperoxidase (proMPO) and the role of the propeptide in processing and maturation. J Biol Chem *292*, 8244-8261.

Harrison, J.E., and Schultz, J. (1976). Studies on the chlorinating activity of myeloperoxidase. Journal of Biological Chemistry *251*, 1371-1374.

Haussermann, K., Young, G., Kukura, P., and Dietz, H. (2019). Dissecting FOXP2 Oligomerization and DNA Binding. Angew Chem Int Ed Engl *58*, 7662-7667.

Hinneburg, H., Chatterjee, S., Schirmeister, F., Nguyen-Khuong, T., Packer, N.H., Rapp, E., and Thaysen-Andersen, M. (2019). Post-Column Make-Up Flow (PCMF) Enhances the Performance of Capillary-Flow PGC-LC-MS/MS-Based Glycomics. Analytical chemistry *91*, 4559-4567.

Hoogendijk, A.J., Pourfarzad, F., Aarts, C.E.M., Tool, A.T.J., Hiemstra, I.H., Grassi, L., Frontini, M., Meijer, A.B., van den Biggelaar, M., and Kuijpers, T.W. (2019). Dynamic Transcriptome-Proteome Correlation Networks Reveal Human Myeloid Differentiation and Neutrophil-Specific Programming. Cell Rep *29*, 2505-2519 e2504.

Hubber, S.J., and Thornton, J.M. (1993). NACCESS computer program. Department of Biochemistry and Molecular Biology, University College, London.

Jensen, P.H., Karlsson, N.G., Kolarich, D., and Packer, N.H. (2012). Structural analysis of N- and O-glycans released from glycoproteins. Nature Protocols *7*, 1299.

Kawahara, R., Ortega, F., Rosa-Fernandes, L., Guimarães, V., Quina, D., Nahas, W., Schwämmle, V., Srougi, M., Leite, K.R.M., Thaysen-Andersen, M.*, et al.* (2018). Distinct urinary glycoprotein signatures in prostate cancer patients. Oncotarget *9*, 33077-33097.

Khalilova, I.S., Dickerhof, N., Mocatta, T.J., Bhagra, C.J., McClean, D.R., Obinger, C., and Kettle, A.J. (2018). A myeloperoxidase precursor, pro-myeloperoxidase, is present in human plasma and elevated in cardiovascular disease patients. PLoS One *13*, e0192952.

Khan, A.A., Alsahli, A.M., and Rahmani, H.A. (2018). Myeloperoxidase as an Active Disease Biomarker: Recent Biochemical and Pathological Perspectives. Medical Sciences *6*.

Kim, H.J., Wei, Y., Wojtkiewicz, G.R., Lee, J.Y., Moskowitz, M.A., and Chen, J.W. (2018). Reducing myeloperoxidase activity decreases inflammation and increases cellular protection in ischemic stroke. Journal of Cerebral Blood Flow & Metabolism, 0271678X18771978.

Klebanoff, S.J. (1968). Myeloperoxidase-Halide-Hydrogen Peroxide Antibacterial System. Journal of Bacteriology *95*, 2131.

Klebanoff, S.J. (2005). Myeloperoxidase: Friend and foe. J. Leukocyte Biol. *77*, 598-625.

Loke, I., Ostergaard, O., Heegaard, N.H.H., Packer, N.H., and Thaysen-Andersen, M. (2017). Paucimannose-Rich N-glycosylation of Spatiotemporally Regulated Human Neutrophil Elastase Modulates Its Immune Functions. Mol Cell Proteomics *16*, 1507-1527.

Loke, I., Packer, N.H., and Thaysen-Andersen, M. (2015). Complementary LC-MS/MS-Based N-Glycan, N-Glycopeptide, and Intact N-Glycoprotein Profiling Reveals Unconventional Asn71-Glycosylation of Human Neutrophil Cathepsin G. Biomolecules *5*, 1832-1854.

Marty, M.T., Baldwin, A.J., Marklund, E.G., Hochberg, G.K.A., Benesch, J.L.P., and Robinson, C.V. (2015). Bayesian Deconvolution of Mass and Ion Mobility Spectra: From Binary Interactions to Polydisperse Ensembles. Analytical chemistry *87*, 4370-4376.

Nauseef, W.M. (1986). Myeloperoxidase biosynthesis by a human promyelocytic leukemia cell line: insight into myeloperoxidase deficiency. Blood *67*, 865.

Nauseef, W.M. (1987). Posttranslational processing of a human myeloid lysosomal protein, myeloperoxidase. Blood *70*, 1143.

Nauseef, W.M. (2014a). Isolation of Human Neutrophils from Venous Blood. In Neutrophil Methods and Protocols, M.T. Quinn, and F.R. DeLeo, eds. (Totowa, NJ: Humana Press), pp. 13-18.

Nauseef, W.M. (2014b). Myeloperoxidase in human neutrophil host defence. Cell Microbiol *16*, 1146-1155.

Nauseef, W.M. (2018). Biosynthesis of human myeloperoxidase. Archives of Biochemistry and Biophysics *642*, 1-9.

Nauseef, W.M., McCormick, S., and Yi, H. (1992). Roles of heme insertion and the mannose-6-phosphate receptor in processing of the human myeloid lysosomal enzyme, myeloperoxidase. Blood *80*, 2622-2633.

Paumann-Page, M., Furtmuller, P.G., Hofbauer, S., Paton, L.N., Obinger, C., and Kettle, A.J. (2013). Inactivation of human myeloperoxidase by hydrogen peroxide. Arch Biochem Biophys *539*, 51-62.

Ravnsborg, T., Houen, G., and Hojrup, P. (2010). The glycosylation of myeloperoxidase. Biochim Biophys Acta *1804*, 2046-2053.

Reiding, K.R., Franc, V., Huitema, M.G., Brouwer, E., Heeringa, P., and Heck, A.J.R. (2019). Neutrophil myeloperoxidase harbors distinct site-specific peculiarities in its glycosylation. Journal of Biological Chemistry.

Rørvig, S., Østergaard, O., Heegaard, N.H.H., and Borregaard, N. (2013). Proteome profiling of human neutrophil granule subsets, secretory vesicles, and cell membrane: correlation with transcriptome profiling of neutrophil precursors. J. Leukocyte Biol. *94*, 711-721.

Samygina, V.R., Sokolov, A.V., Bourenkov, G., Petoukhov, M.V., Pulina, M.O., Zakharova, E.T., Vasilyev, V.B., Bartunik, H., and Svergun, D.I. (2013). Ceruloplasmin: macromolecular assemblies with iron-containing acute phase proteins. PloS one *8*, e67145-e67145.

Silvescu, C.I., and Sackstein, R. (2014). G-CSF induces membrane expression of a myeloperoxidase glycovariant that operates as an E-selectin ligand on human myeloid cells. Proc Natl Acad Sci U S A *111*, 10696-10701.

Soltermann, F., Foley, E., Pagnoni, V., Galpin, M., Benesch, J., Kukura, P., and Struwe, W. (2020). Quantifying protein-protein interactions by molecular counting with mass photometry. Angew Chem Int Ed Engl.

Stamp, L.K., Khalilova, I., Tarr, J.M., Senthilmohan, R., Turner, R., Haigh, R.C., Winyard, P.G., and Kettle, A.J. (2012). Myeloperoxidase and oxidative stress in rheumatoid arthritis. Rheumatology *51*, 1796-1803.

Takeuchi, K., Umeki, Y., Matsumoto, N., Yamamoto, K., Yoshida, M., Suzuki, K., and Aratani, Y. (2012). Severe neutrophil-mediated lung inflammation in myeloperoxidase-deficient mice exposed to zymosan. Inflammation Research *61*, 197-205.

Thaysen-Andersen, M., and Packer, N.H. (2012). Site-specific glycoproteomics confirms that protein structure dictates formation of N-glycan type, core fucosylation and branching. Glycobiology *22*, 1440-1452.

Thaysen-Andersen, M., Packer, N.H., and Schulz, B.L. (2016). Maturing Glycoproteomics Technologies Provide Unique Structural Insights into the N-glycoproteome and Its Regulation in Health and Disease. Mol Cell Proteomics *15*, 1773-1790.

Thaysen-Andersen, M., Venkatakrishnan, V., Loke, I., Laurini, C., Diestel, S., Parker, B.L., and Packer, N.H. (2015). Human Neutrophils Secrete Bioactive Paucimannosidic Proteins from Azurophilic Granules into Pathogen-Infected Sputum. The Journal of Biological Chemistry *290*, 8789-8802.

Tjondro, H.C., Loke, I., Chatterjee, S., and Thaysen-Andersen, M. (2019). Human protein paucimannosylation: cues from the eukaryotic kingdoms. Biol Rev Camb Philos Soc *94*, 2068-2100.

Van Antwerpen, P., Slomianny, M.C., Boudjeltia, K.Z., Delporte, C., Faid, V., Calay, D., Rousseau, A., Moguilevsky, N., Raes, M., Vanhamme, L.*, et al.* (2010). Glycosylation pattern of mature dimeric leukocyte and recombinant monomeric myeloperoxidase: glycosylation is required for optimal enzymatic activity. J Biol Chem *285*, 16351-16359.

Vanhamme, L., Zouaoui Boudjeltia, K., Van Antwerpen, P., and Delporte, C. (2018). The other myeloperoxidase: Emerging functions. Archives of Biochemistry and Biophysics *649*, 1-14.

Varki, A., Cummings, R.D., Aebi, M., Packer, N.H., Seeberger, P.H., Esko, J.D., Stanley, P., Hart, G., Darvill, A., Kinoshita, T.*, et al.* (2015). Symbol Nomenclature for Graphical Representations of Glycans. Glycobiology *25*, 1323-1324.

Venkatakrishnan, V., Dieckmann, R., Loke, I., Tjondro, H., Chatterjee, S., Bylund, J., Thaysen-Andersen, M., Karlsson, N.G., and Karlsson-Bengtsson, A. (2020). Glycan analysis of human neutrophil granules implicates a maturation-dependent glycosylation machinery. J Biol Chem.

Wang, J., Li, J.N., Cui, Z., and Zhao, M.H. (2018). Deglycosylation influences the oxidation activity and antigenicity of myeloperoxidase. Nephrology (Carlton) *23*, 46-52.

Winterbourn, C.C., Kettle, A.J., and Hampton, M.B. (2016). Reactive Oxygen Species and Neutrophil Function. Annu Rev Biochem *85*, 765-792.

Young, G., Hundt, N., Cole, D., Fineberg, A., Andrecka, J., Tyler, A., Olerinyova, A., Ansari, A., Marklund, E.G., Collier, M.P.*, et al.* (2018). Quantitative mass imaging of single biological macromolecules. Science *360*, 423-427.

Yu, J.T., Li, J.N., Wang, J., Jia, X.Y., Cui, Z., and Zhao, M.H. (2017). Deglycosylation of myeloperoxidase uncovers its novel antigenicity. Kidney Int *91*, 1410-1419.

Figure 1

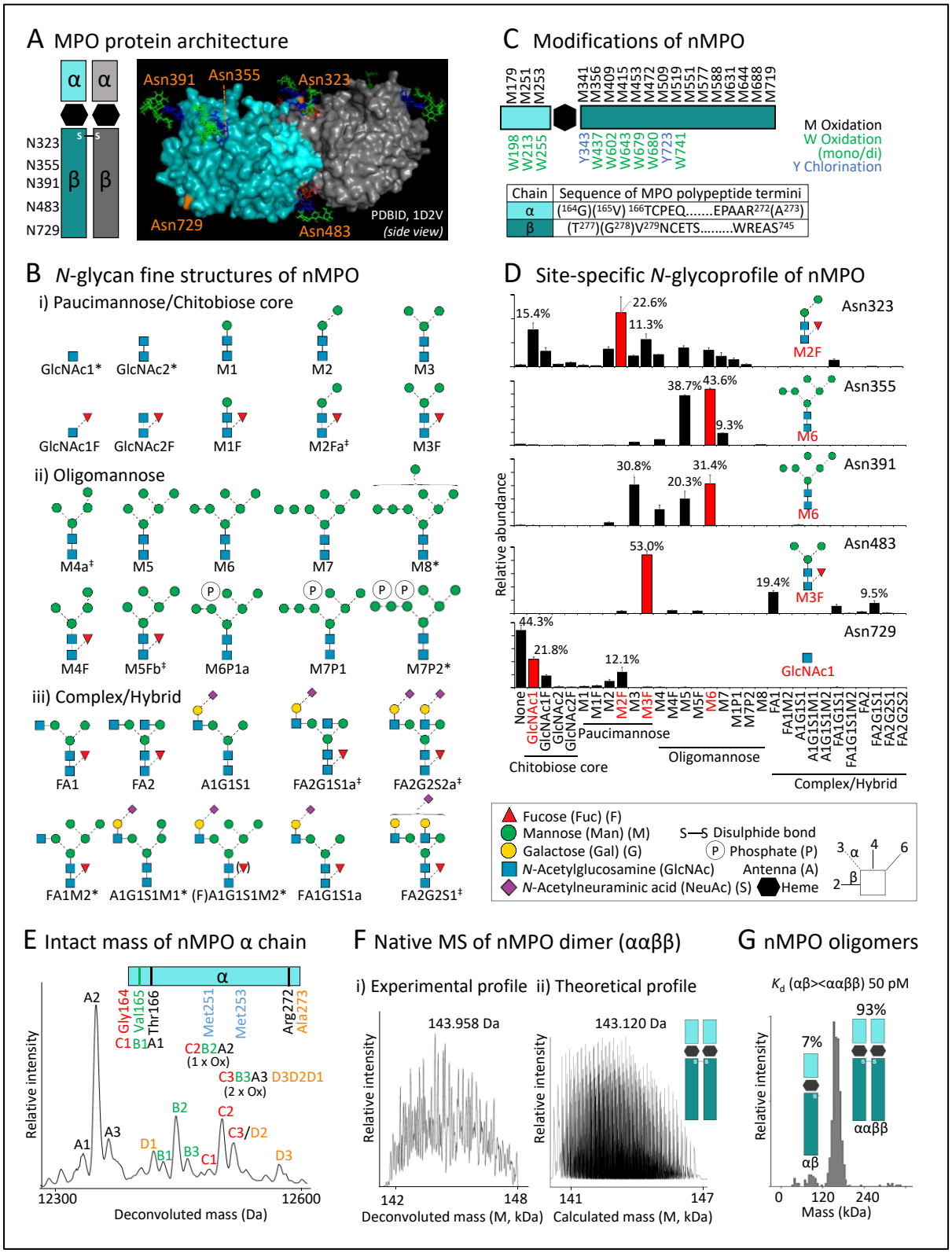

Figure 1. Deep structural characterisation of neutrophil-derived myeloperoxidase (nMPO). A) Protein architecture of MPO, a heme-containing diprotomer (ααββ) (left). Each β-chain harbours five sequons (orange) here mapped on dimeric MPO (PDBID, 1D2V). Asn729 was left unoccupied while

characteristic glycans were added *in silico* to other sites (see D). **B**) Fine structures and short-hand nomenclature of the nMPO *N*-glycans (**Supplementary Figure S1, Supplementary Table S6** and **Supplementary Data S1**). *Several additional hyper-truncated and/or trace *N*-glycans were observed at the peptide level. ‡Multiple glycan isomers (designated a, b..) were identified. See key for glycan symbol nomenclature and linkage representation (Varki et al., 2015). **C**) Non-glycan modifications of nMPO including Met (black) and Trp (green) mono- and di-oxidation, Tyr (blue) mono-chlorination and polypeptide truncation variants (**Supplementary Figure S2** and **Supplementary Data S2A-B**). **D**) Site-specific *N*-glycoprofile of nMPO (**Supplementary Figure S3, Supplementary Table S7** and **Supplementary Data S3A-E**). Prominent *N*-glycans at each site are in red. Data plotted as mean ± SD, n = 3, technical replicates. **E**) Intact mass analysis revealed limited α-chain heterogeneity arising from polypeptide truncation and oxidation variants, presumably Met251 and Met253, as supported by peptide data (**Supplementary Table S3A**). **F**) i-ii) Native MS demonstrated extreme complexity of the dimeric nMPO (ααββ) that matched the expected profile generated from approximately 300,000 predicted proteoforms (**Supplementary Table S3B**). **G**) Mass photometry revealed the existence of both a low-abundance monomer (7%) and high-abundance dimer (93%) of nMPO.

Figure 2

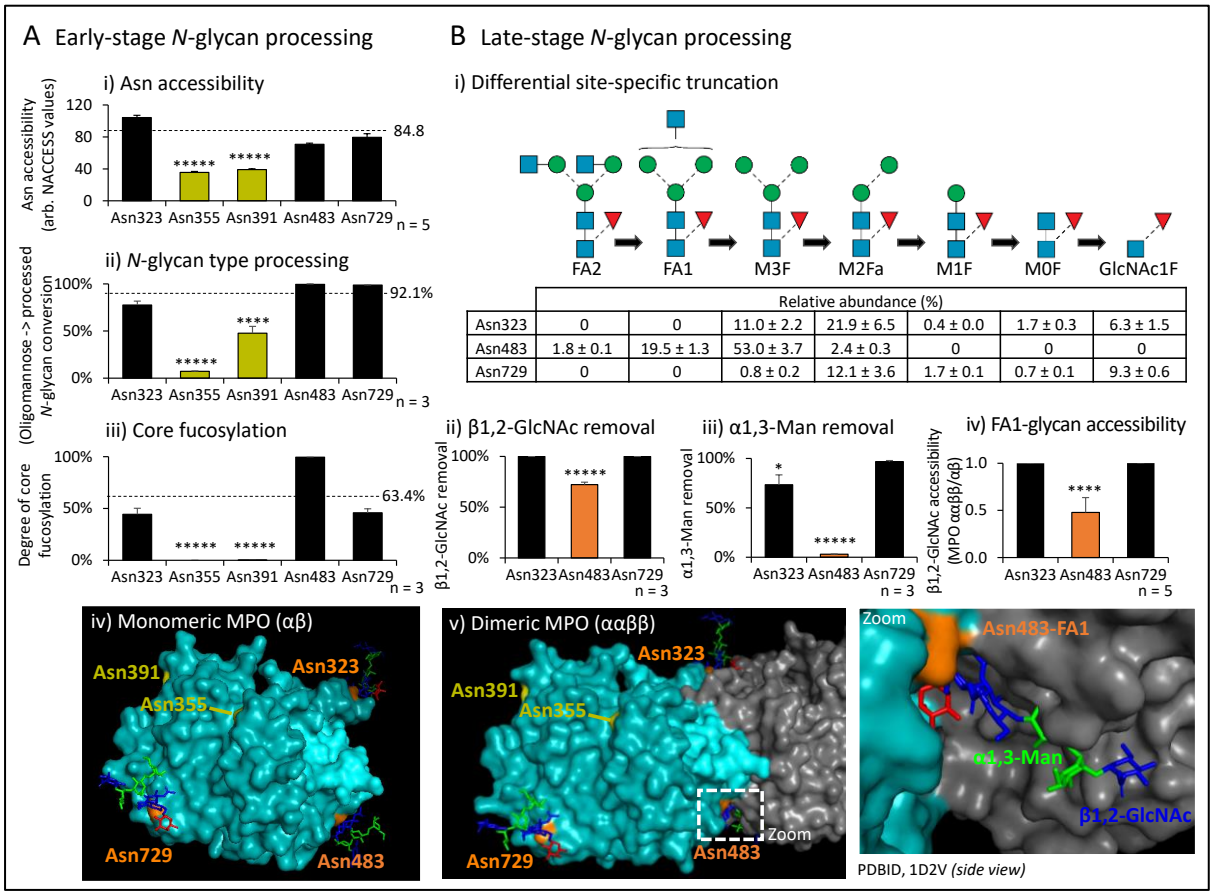

Figure 2. Solvent accessibility and oligomerisation impact the local *N*-glycan processing of MPO. **A**) Investigation of maturely folded monomeric MPO (as it appears in the early-stage processing) revealed a correlation between i) the Asn accessibility and the degree of ii) *N*-glycan type processing plotted as the oligomannose-to-processed *N*-glycan conversion, and iii) core fucosylation determined from possible FUT8 substrates based on nMPO glycopeptide profiling and solvent accessibility data (**Figure 1D, Supplementary Table S7** and **Supplementary Table S8A**). The inaccessible Asn355 and Asn391 (green bars) carried mostly under-processed oligomannosidic *N*-glycans and afucosyated *N*-glycans. Mean values for the accessible sites (Asn323, Asn483, Asn729) (broken lines) were used for statistical comparisons to Asn355 and Asn391. iv) Inaccessible Asn355 and Asn391 (green, depicted without glycans for clarity) and accessible Asn323, Asn729 and Asn483 (orange) were mapped on monomeric MPO (PDBID, 1D2V). **B**) i) Exploration of the late-stage glycan processing of maturely folded MPO involving the *N*-glycan truncation pathway (Tjondro et al., 2019) demonstrated less truncation of the Asn483-glycans and partly Asn323-glycans as measured by the lower removal efficiency of terminal residues including ii) β1,2-GlcNAc and iii) α1,3-Man residues relative to Asn729-glycans based on nMPO glycopeptide data and iv) a reduced β1,2-GlcNAc accessibility of FA1-conjugated Asn483 (orange) upon MPO dimerisation (**Supplementary Table S8B**). Statistical comparisons were made to

Asn729. v) Illustration of the dimerisation-dependent occlusion of the Asn483-glycan on dimeric MPO (1D2V). Contact between (and hence masking of) the Asn483-FA1 glycan and the protein surface of the other αβ-protomer was observed (see zoom). The Asn323-glycan positioned near the dimer interface was partially affected by MPO dimerisation. For all panels, data plotted as mean ± SD, n = 3 (glycopeptide profiling), n = 5 (solvent accessibility), *$p < 0.05$, **$p < 0.01$, ***$p < 0.005$, ****$p < 0.001$, *****$p < 0.00005$. See **Figure 1** for colour coding of MPO and glycan nomenclature.

Figure 3

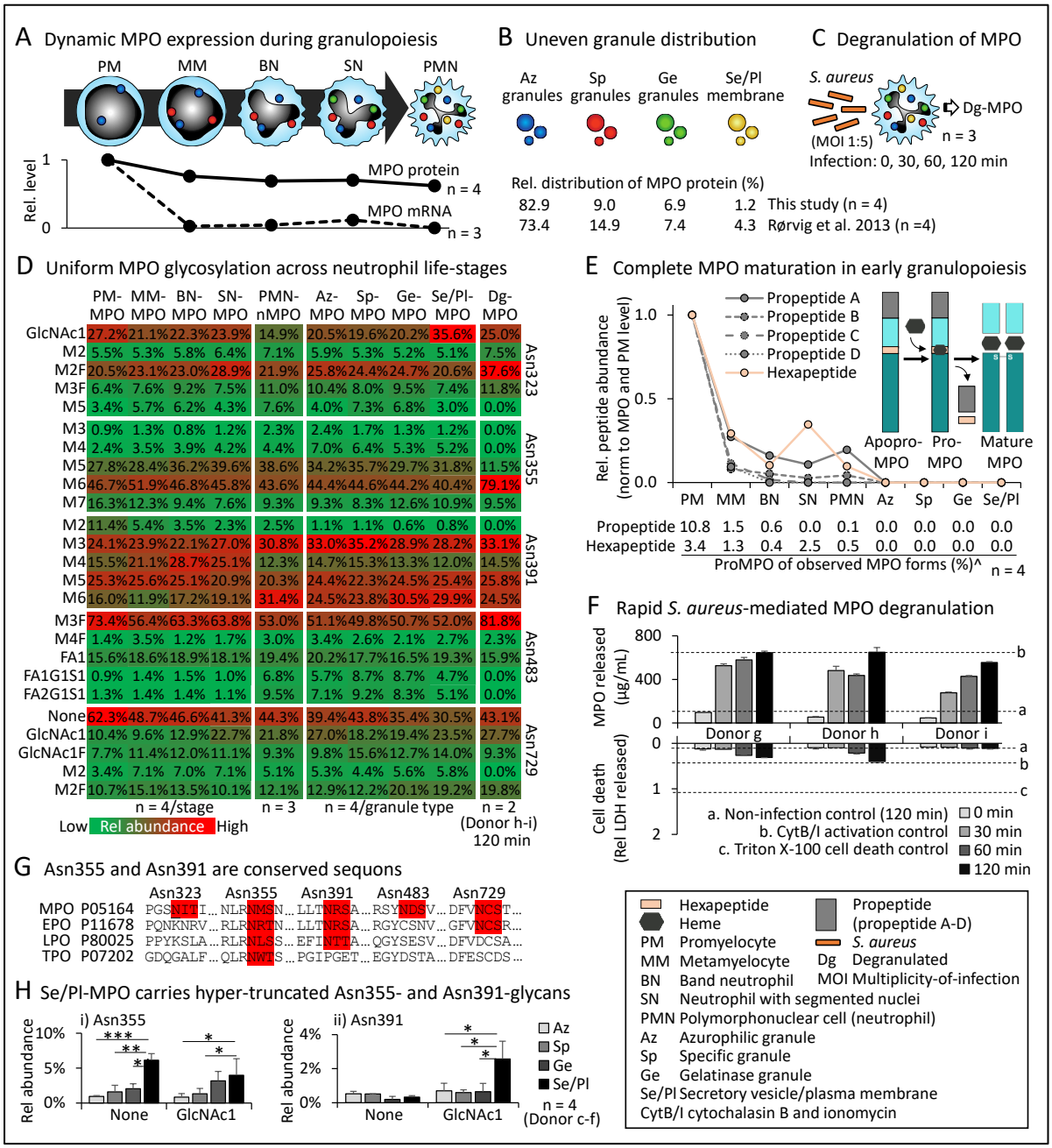

Figure 3. **Dynamics, granule distribution, polypeptide processing, site-specific glycosylation, and degranulation of MPO across the neutrophil life stages**. **A**) Dynamic expression of MPO mRNA and protein during granulopoiesis. Relative MPO expression levels, normalised to the PM-stage, were based on data re-interrogation (Hoogendijk et al., 2019). See key for nomenclature. **B**) Quantitative proteomics of granule-separated neutrophils showed an uneven MPO distribution across granules congruent with the literature (Rørvig et al., 2013). **C**) *S. aureus*-mediated neutrophil activation. Longitudinal profiling of the levels and glycosylation of released Dg-MPO was performed (see Panel F and D for data and controls). **D**) Site-specific glycoprofiling of MPO from maturing, resting (PMN-

nMPO, see Figure 1D), granule-separated, and activated neutrophils. Prominent *N*-glycans at each site were plotted (**Supplementary Figure S5** and **Supplementary Table S10**). The MPO glycosylation of maturing neutrophils was determined from data re-analysis (Hoogendijk et al., 2019). Heat intensity scale and biological replicates are indicated. See **Figure 1** for short-hand nomenclature of glycans. **E**) Longitudinal tracking of MPO polypeptide processing (proMPO-to-MPO conversion) within maturing, mature, and granule-separated neutrophils. Relative levels of peptides arising from the proMPO regions (normalised to PM-stage) were plotted. ^ProMPO levels were determined from the intensity of related peptides arising from proMPO and mature MPO. The data did not allow distinction between apoproMPO and proMPO. See insert for schematics of MPO polypeptide maturation. **F**) *S. aureus*-mediated activation of neutrophils (MOI 1:5) demonstrating a rapid time-dependent and cell death-independent degranulation of Dg-MPO as measured by ELISA and LDH release assays. Controls (a-c, mean plotted as broken lines) were included for both assays. **G**) Sequence alignment showed that Asn355 and Asn391 are conserved sequons across the human peroxidases implying functional importance (see **Supplementary Figure S6** for alignment to mammalian MPO). **H**) Hyper-truncated GlcNAcβAsn and absence of glycosylation were elevated features at i) Asn355 and ii) Asn391 of Se/Pl-MPO relative to MPO from other granules. For all panels, data plotted as mean ± SD. ns, not significant ($p \geq 0.05$), *$p < 0.05$, **$p < 0.01$, ***$p < 0.005$, ****$p < 0.001$, *****$p < 0.00005$.

Figure 4

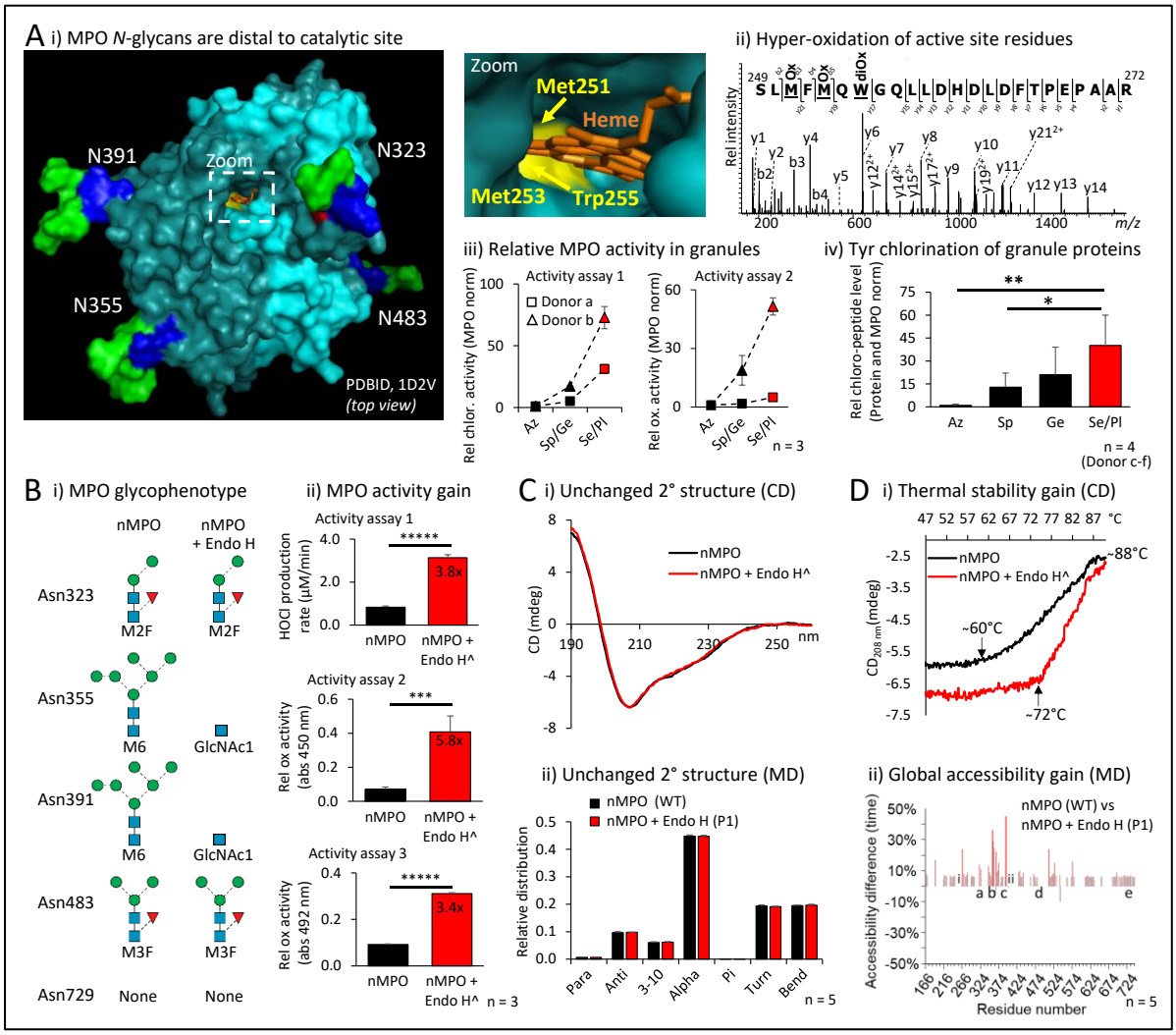

Figure 4. **Hyper-truncated Asn355- and Asn391-GlcNAc signatures positioned distal to the catalytic site augment the MPO activity**. **A**) i) The MPO *N*-glycans are distal to the catalytic site. Zoom: Oxidation-prone Met251, Met253 and Trp255 (yellow) in the heme-containing (orange) catalytic site. Mapped on monomeric MPO (PDBID, 1D2V), see **Figure 1** for MPO colour coding and key to glycans. ii) Hyper-oxidation of Met251, Met253 and Trp255 indicates extensive self-oxidation, which may impact MPO activity by reconfiguration of the active site. iii) Se/Pl-MPO from Donor a-b displayed a higher chlorination and oxidation activity than MPO from other granules (**Supplementary Table S11**). Adjusted for MPO level, n = 3, technical replicates. iv) Relative Tyr chlorination level of proteins from granules fractionated with high resolution of neutrophils from Donor c-f (**Supplementary Table S12**). Adjusted for total protein and MPO level, n = 4 biological replicates. **B**) i) Endoglycosidase H (Endo H)-treatment of nMPO produced a Asn355- and Asn391-GlcNAc glycophenotype (mimicking enriched GlcNAcβAsn signatures of Se/Pl-MPO, see **Figure 3H**) as validated using LC-MS/MS (**Figure 5B** and **Supplementary Figure S7**). Main glycoforms are shown for each site. ii) The Endo H-treated nMPO

exhibited a higher enzyme activity than untreated nMPO based on measurements of HOCl production (activity assay 1) and the oxidation rate (activity assays 2-3). For all assays, n = 3, technical replicates (**Supplementary Table S5A-C**). **C**) Endo H-treated and untreated nMPO displayed indistinguishable secondary structure profiles based on i) CD profiling (see **Supplementary Table S13A-B**) and ii) MD-based predictions. **D**) Relative to untreated nMPO (WT), Endo H-treated MPO (P1) showed i) higher thermal stability as determined by $CD_{208\ nm}$ (arrows indicate the initial melting temperatures) and ii) greater global polypeptide accessibility based on MD data (see **Supplementary Figure S8-9**). Key: a-e and i-ii indicate positions of the MPO glycosylation sites and key catalytic residues, respectively. For panel Bii, Ci, and Di: ^Data from Endo H only controls were subtracted from Endo H-treated nMPO data to enable comparison to untreated nMPO. For all panels: Data plotted as mean ± SD, ns, not significant ($p \geq 0.05$), *$p < 0.05$, **$p < 0.01$, ***$p < 0.005$, ****$p < 0.001$, *****$p < 0.00005$.

Figure 5

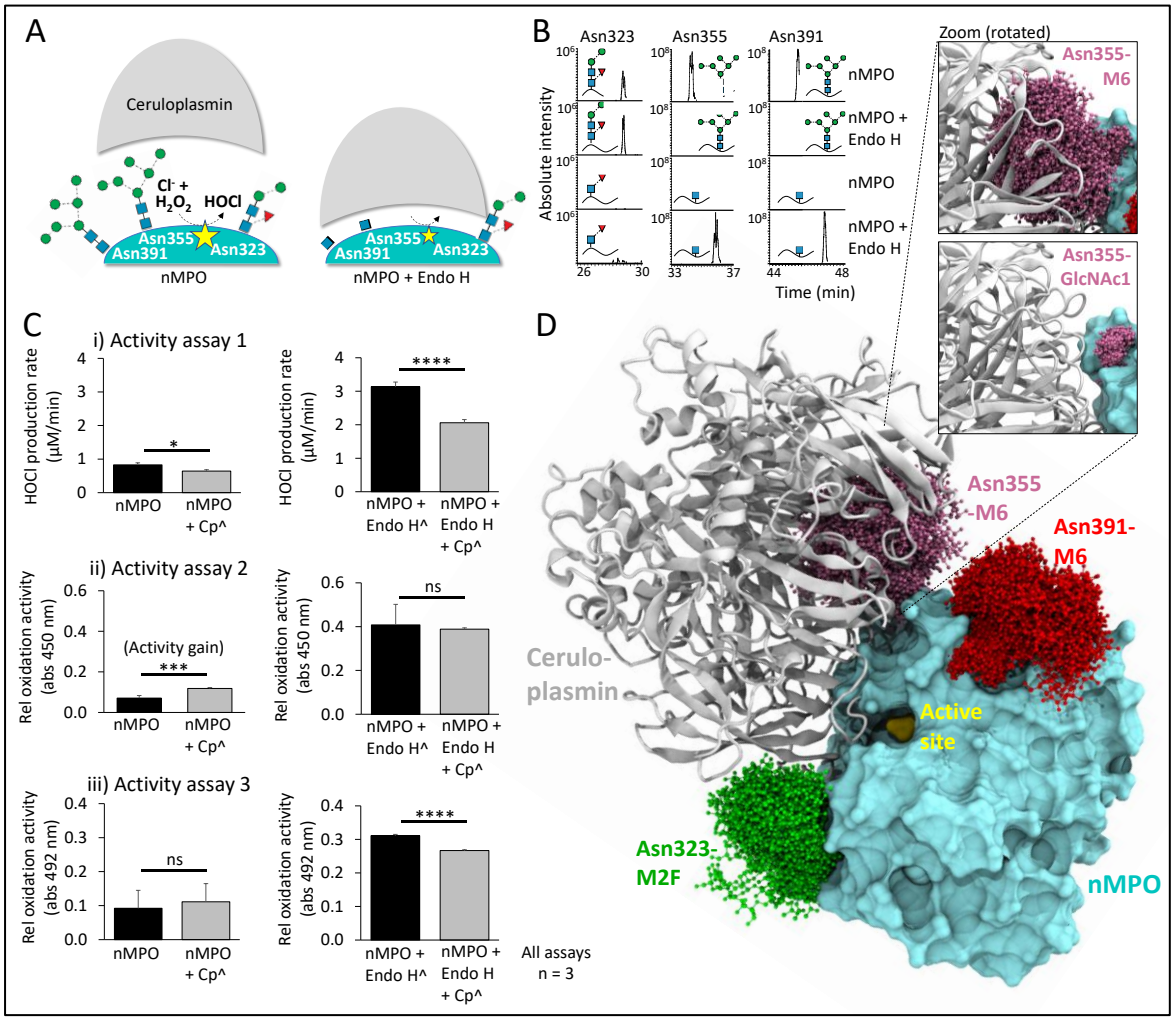

Figure 5. Hyper-truncated Asn355-glycosylation promotes ceruloplasmin-mediated MPO inhibition. **A**) Schematics of the glycoform-dependent ceruloplasmin-based inhibition of Endo H-treated and untreated nMPO. Common glycans decorating Asn323, Asn355, and Asn391 in proximity to the MPO-ceruloplasmin interface and the HOCl-producing active site (yellow star) are portrayed. **B**) Glycopeptide data (selected EICs) demonstrating a complete conversion of Asn355-M6 and Asn391-M6 to GlcNAcβAsn upon Endo H-treatment (**Supplementary Figure S7**). The Endo H-insensitive Asn323-M2F was included as a control. **C**) The chlorination (i) and relative oxidation (ii-iii) levels of untreated nMPO (left graphs) and Endo H-treated nMPO (right) incubated with (grey bars) and without (black) serum-derived ceruloplasmin (denoted Cp) were determined using activity assay 1-3, respectively (**Supplementary Table S5D-F**). n = 3, technical replicates. **D**) Modelling using a structure of the ceruloplasmin-MPO complex (PDBID, 4EJX) and MD data of Asn323-M2F (green), Asn355-M6 (magenta) and Asn391-M6 (red) of nMPO proximal to the interface demonstrated that Asn355-M6 and not Asn355-GlcNAc clashes with ceruloplasmin (see slightly rotated zoom). Data plotted as mean ± SD, ns, not significant ($p \geq 0.05$), *$p < 0.05$, **$p < 0.01$, ***$p < 0.005$, ****$p < 0.001$.